4 Fundamental studies: Process understanding on a molecular scale

Fundamental studies on radionuclide chemistry and geochemistry are performed at KIT-INE in order to develop detailed scientific understanding on a molecular scale and ensure the reliable quantitative prediction of key processes in aquatic chemistry. Aiming at a comprehensive assessment of radionuclide behavior and mobility in aquatic systems relevant for the Nuclear Waste Disposal Safety Case, experimental studies with actinides and long-lived fission products are performed. The investigated aqueous systems range from dilute solutions to highly saline salt brine systems and establish essential site-independent data and scientific process understanding. Work is focusing both on detailed experimental investigations using the unique facilities available at KIT-INE, and subsequently developing reliable chemical models and consistent thermodynamic data. This combined approach allows a systematic and reliable evaluation of key processes such as radionuclide solubility, radionuclide speciation, radionuclide retention and transport processes in relevant near- and far-field scenarios.

The work summarized in this section is related to the (i) chemistry and thermodynamics of actinides and fission products in aqueous solution, (ii) radionuclide sorption on mineral phases, and (iii) retention of radionuclides by secondary phase formation. The studies aim at identifying relevant radionuclide retention/retardation mechanisms on a molecular level and their robust thermodynamic quantification in support of the Nuclear Waste Disposal Safety Case. The fundamental studies on aqueous radionuclide chemistry described in Chapter 4 are using radionuclide speciation methods developed at KIT-INE (see Chapter 8), and support the applied studies performed at KIT-INE (see Chapter 5).

4.1 Chemistry and thermodynamics of actinides and fission products in aqueous solution

N. Adam, M. Altmaier, A. Baumann, M. Böttle, N. Cevirim, K. Dardenne, F. Endrizzi, D. Fellhauer,
D. R. Fröhlich, X. Gaona, J.-Y. Lee, P.J. Panak, R. Polly, J. Rothe, J. Schepperle, A. Skerencak-Frech, A. Tasi,
M. Trumm, E. Yalcintas

In co-operation with:

J. Bruno[a], E. Colàs[a], M. Grivé[a], A. Johnsen[b], K. Källström[c]

[a] Amphos[21] Consulting S.L., Passeig Garcia i Faria, 49-51, 1-1a, 08019 Barcelona, Spain; [b] Penn State University, Radiation Science and Engineering Center, 101 Breazeale Nuclear Reactor, University Park, PA 16802, USA; [c] Svensk Kärnbränslehantering AB, Avd. Låg-och medelaktivt avfall, Box 250, 101 24 Stockholm, Sweden

Introduction

Aquatic chemistry and thermodynamics of actinides and fission products is a multifold and scientifically challenging field of inorganic chemistry. The research activities developed at KIT-INE within this field mainly focus on systems relevant for nuclear waste disposal, and aim at contributing to the Safety Case and Performance Assessment of repositories designed for the disposal of such wastes. This section highlights the fundamental and applied research performed at KIT-INE in 2016 within this topic.

In the context of aquatic chemistry and thermodynamics, KIT-INE contributes to several national projects with focus on the interdisciplinary analyses of disposal options for radioactive waste (ENTRIA, funded by BMBF), providing support and expert judgement to BfS with regard to geochemical processes of relevance in the Asse II salt mine, or participating in the development of the national thermodynamic reference database for actinides and fission products (THEREDA project). The leading role of KIT-INE in this field is further reflected in key contributions to highly relevant international projects, such as the OECD NEA-TDB thermodynamic series, the IUPAC Subcommittee on Solubility and Equilibrium Data, or the update of the Plutonium Handbook edited by the American Nuclear Society, among others.

Tc(IV) solubility and carbonate complexation in alkaline, dilute to concentrated saline systems

Technetium-99 is one of the main fission products of ^{235}U and ^{239}Pu produced in nuclear reactors. Due to its long half-life ($2.1 \cdot 10^5$ a) and redox-sensitive character, ^{99}Tc is a very relevant radionuclide in the Safety Assessment of nuclear waste repositories. Tc(VII) is the prevailing oxidation state under oxidizing and redox-neutral conditions and exists as soluble and mobile TcO_4^-. On the contrary, Tc(IV) forms sparingly soluble hydrous oxides ($TcO_2 \cdot xH_2O(s)$) under reducing conditions as those expected in deep underground repositories. Carbonate is an important component in the pore water of certain host-rocks, and is known to form strong complexes with metal cations, potentially contributing to the mobilization of radionuclides. In this context, an appropriate understanding of Tc(IV) solubility and aqueous speciation in alkaline car-

bonate-containing solutions provides relevant inputs for assessing the behavior of Tc in underground repositories for radioactive waste disposal.

The solubility of Tc(IV) was investigated in carbonate-containing solutions of varying ionic strength (I = 0.5 - 5.0 M) and at different pH_m (-log [H^+] = 8.5 - 14.5). The experiments were split in three independent series: (i) constant ionic strength I = 5.0 M ($NaCl$-$NaHCO_3$-Na_2CO_3) with total carbonate concentration (C_{tot} = [HCO_3^-] + [CO_3^{2-}]) 0.01 M $\leq C_{tot} \leq$ 0.5 M and 8.5 $\leq pH_m \leq$ 12.0, (ii) constant C_{tot} = 0.05 and 0.1 M with 0.5 M $\leq I \leq$ 5.0 M ($NaCl$-$NaHCO_3$-Na_2CO_3) and 8.5 $\leq pH_m \leq$ 12.0, (iii) constant C_{tot} = 0.1, 0.5 and 1.0 M with 0.01 M $\leq$ [$NaOH$] $\leq$ 0.6 M (in the absence of $NaCl$). $SnCl_2$ was used as reducing agent to ensure that Tc both as solid and in solution remains in oxidation state +IV. [Tc], pH_m and E_h were monitored at regular time intervals. The redox state of Tc in the aqueous phase was investigated for selected samples by XANES/EXAFS spectroscopy and solvent extraction with TPPC. Density functional theory (DFT) calculations were performed to identify the most stable structure of the Tc(IV)-CO_3 complexes forming in alkaline pH conditions.

A strong effect of carbonate was observed in all investigated samples, leading to up to 3 orders of magnitude greater solubility than in carbonate-free systems (see Figure 1).

XANES and solvent extraction confirmed that Tc(IV) prevails in the aqueous phase of the investigated systems, and thus that the increase in solubility is not caused by the oxidation to Tc(VII). Solubility data collected at 9 $\leq pH_m \leq$ 12 are properly explained with the equilibrium reaction $TcO_2 \cdot 0.6H_2O(s)$ + CO_3^{2-} + 0.4 $H_2O(l)$ + H^+ $\Leftrightarrow$ $TcCO_3(OH)_3^-$, although thermodynamic data selected in the NEA-TDB for this complex significantly underestimates the experimental results obtained in the present study [1].
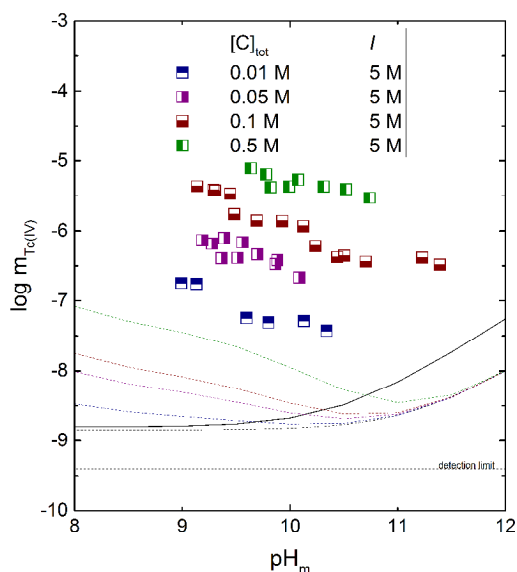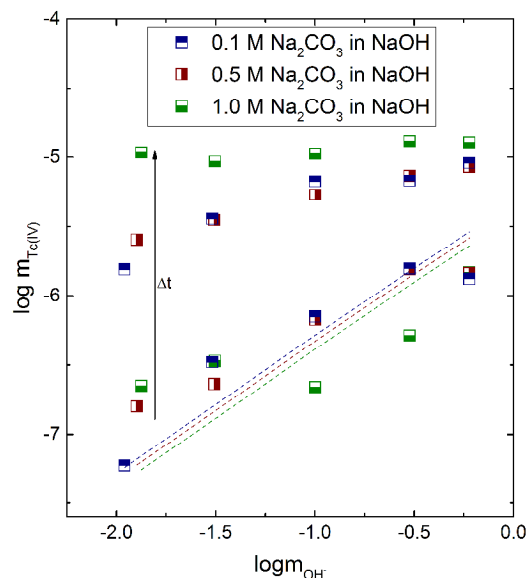
Fig. 2: Experimental solubility data of Tc(IV) in carbonate systems (symbols), and calculated solubility using thermodynamic and activity models reported in [1–3] (dashed lines).

Above $pH_m \approx$ 12, the increased Tc(IV) solubility with respect to carbonate-free systems may hint to the formation of the so far unreported complex $TcCO_3(OH)_4^{2-}$ (see Figure 2), although further experimental evidences are needed to confirm this hypothesis. DFT calculations point to the stabilization of hydrated carbonate hydroxo complexes ($TcCO_3(OH)_x^{2-x}$) over oxo-hydroxo complexes ($TcOCO_3(OH)_y^{y-}$) containing the moiety TcO^{2+}. The systematic and very comprehensive solubility dataset obtained for Tc(IV) in alkaline carbonate-containing solutions allows deriving accurate chemical, thermodynamic and activity (SIT) models for the system Tc^{4+}-H^+-Na^+-CO_3^{2-}-HCO_3^--OH^--Cl^--$H_2O(l)$. These models are highly relevant in geochemical calculations and for the estimation of reliable Tc(IV) source term concentrations in the context of safety assessments for nuclear waste repositories.

U(IV) hydrolysis and carbonate complexation in dilute to concentrated salt systems

Uranium is the main element in the nuclear fuel cycle and, consequently, contributes with the largest inventory to radioactive waste. U(VI) is the most stable oxidation state of uranium under anoxic and oxidizing conditions, whereas U(IV) prevails in strongly reducing environments, forming the sparingly soluble UO_2(am,hyd) in the absence of complexing ligands. The predominance of the latter oxidation state is expected in underground repositories, where very reducing conditions are expected due to the anoxic corrosion of steel. The geochemical boundary conditions of aqueous solutions potentially contacting nuclear waste may contain low to high concentrations of dissolved salts (I = 0.1 M - 15 M) as well as strong complexing ligands like CO_3^{2-}, which can significantly alter the

Fig. 1: Experimental solubility data of Tc(IV) in carbonate systems with I = 5 M (symbols), and calculated solubility using thermodynamic and activity models reported in [1–3] (dashed lines).

chemical behavior of uranium and therefore impact its retention/migration processes. In this framework, an appropriate understanding of the solubility, hydrolysis and carbonate complexation of U(IV) in dilute to concentrated saline systems is a relevant contribution to the Performance Assessment of repositories for nuclear waste.

The solubility of uranium was investigated in 0.1, 0.5, 2.0, 5.0 M NaCl-NaOH solutions at $1 \leq \text{pH}_m \leq 14.5$ using an undersaturation approach. The solubility of U(IV) in the presence of carbonate was investigated as a function of carbonate concentration (C_{tot} = 0.01 M - 1.5 M), ionic strength (C_{tot} = 0.1 M - 0.3 M, I = 0.5 M - 4.0 M (NaCl-NaHCO$_3$-Na$_2$CO$_3$)) and hydroxide concentration (C_{tot} = 0.1, 0.01 M $\leq$ [NaOH] $\leq$ 0.6 M). All experiments were performed in Ar gloveboxes at T = (22 ± 2)°C. Reducing conditions were chemically controlled with Sn(II) resulting in (pe + pH$_m$) ≈ 2. Approximately 5 mg of U(IV) was added to each sample. [U], pH$_m$ and E_h values were monitored at regular time intervals. Thermodynamic equilibrium was assumed after repeated measurements with constant [U] and pH$_m$. After attaining equilibrium conditions, solid phases of selected batch experiments were characterized by XANES/EXAFS analyses.

Figure 3 shows the solubility of UO$_2$(am,hyd) in the absence of carbonate. Two distinct regions can be identified: I. steep decrease of [U] at pH$_m$ ≤ 3, which is attributed to the predominance in solution of U(OH)$_x^{4-x}$ cationic hydrolysis species with $x \leq 3$. The solubility in this pH-region shows the same trend but falls well below the solubility curve of UO$_2$(am,hyd) calculated using thermodynamic data reported in [1] and [4], indicating a higher degree of crystallinity of the solid phase used in the present study; II. all [U] measured above pH$_m$ ≈ 3 and up to pH$_m$ = 14.5 are at the detection limit of ICP-MS (10^{-9} to 10^{-8} M, depending upon salt concentration and dilution factor).

The present observations give no indication for the formation of U^{IV}(OH)$_5^-$ and U^{IV}(OH)$_6^{2-}$ hydrolysis
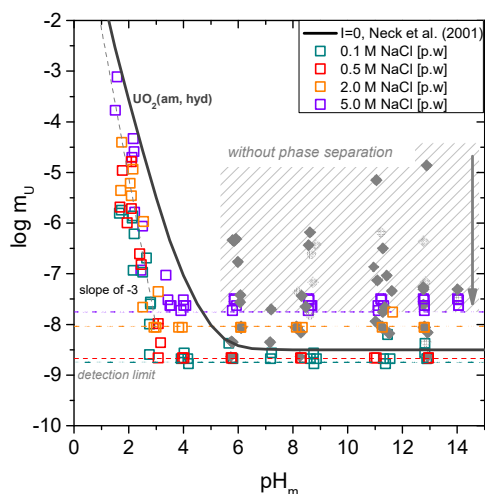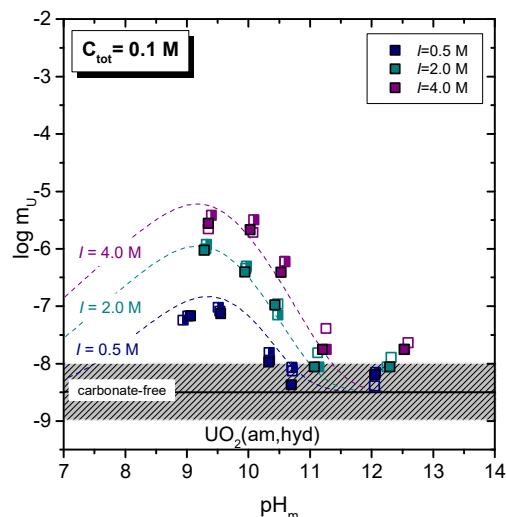
Fig. 4: *Solubility of U(IV) in 0.5, 2.0 and 5.0 M NaCl–NaHCO$_3$–Na$_2$CO$_3$ solutions with C_{tot} = 0.1 M. Dashed lines correspond to UO$_2$(am,hyd) solubility considering the formation of species U(OH)$_2$(CO$_3$)$_3^{4-}$.*

species within the investigated boundary conditions. Increased [U] were measured for samples in region II without phase separation, indicating the presence of U(IV) intrinsic colloids. The U(IV) colloidal fraction decreased with time, eventually reaching the detection limit of ICP-MS after $t \approx 205$ days.

Figure 4 shows the solubility of UO$_2$(am,hyd) in 0.5, 2.0 and 4.0 M NaCl-NaHCO$_3$-Na$_2$CO$_3$ solutions with C_{tot} = 0.1 M. Solubility data at $8.5 \leq \text{pH}_m \leq 11$ in carbonate solutions is up to three orders of magnitude higher than carbonate-free systems. Changes in the solubility suggest the formation of ternary U(IV)-OH-CO$_3$ species in this pH region. No effect of carbonate on the solubility is observed at pH$_m$ ≥ 12, expectedly due to the strong hydrolysis of U(IV). Figure 4 shows also preliminary chemical, thermodynamic and activity models derived in the present work for the system U^{4+}-Na$^+$-H$^+$-Cl$^-$-HCO$_3^-$-CO$_3^{2-}$-OH$^-$-H$_2$O(l). Solubility data above pH$_m$ ≈ 8.5 can be properly explained by defining U(OH)$_2$(CO$_3$)$_3^{4-}$ and U(OH)$_4$(aq) as the predominant aqueous species in equilibrium with UO$_2$(am,hyd).

Solubility and redox behavior of Pu in the presence of ISA and Ca under alkaline, reducing conditions

The final repository for short-lived low- and intermediate-level (L/ILW) nuclear waste in Sweden (SFR) is located in a crystalline host rock formation near Forsmark. Groundwater is expected to slowly intrude from the surrounding rock and saturate the repository in the post-operational phase. Cementitious materials present in SFR will buffer the pH in the alkaline range ($10 \leq \text{pH} \leq 13.3$) over a very long time-scale, whereas strongly reducing conditions are expected to develop as a result of the anaerobic corrosion of the steel containers.

Residual amounts of plutonium present in the inventory of SFR contribute to the long-term radiological

Fig. 3: *Solubility of U(IV) in 0.1, 0.5, 2.0, and 5.0 M NaCl solutions. Solid line corresponds to the solubility curve of UO$_2$(am, hyd) calculated for $I = 0$ using thermodynamic data reported in [1, 4].*

risk potentially arising from the waste due to the long half-life of [239]Pu ($t_{1/2}$ [239]Pu = 2.41·10^4 a) [5]. In reducing aqueous environments, the formation of Pu(III) and Pu(IV) is expected [6]. However, uncertainties in the available thermodynamic data lead to a rather ill-defined redox transition border, especially under alkaline to hyperalkaline conditions [1, 6]. Cellulose is disposed of in large quantities along with L/ILW in SFR [5]. Iso-saccharinic acid (ISA) is the main degradation product of cellulose under hyperalkaline pH conditions defined by cementitious systems [7]. The strong complexation of ISA with An(III) and An(IV) [8] together with the large inventory of this organic ligand present in SFR requires dedicated research efforts with focus on the Pu-ISA-cement system, for which almost no experimental studies are available in the literature.

All experiments were conducted in Ar glove boxes at $T = (22 ± 2)°C$ with O$_2$ concentration below 2 ppm. Independent undersaturation solubility experiments were prepared with 0.2 - 2 mg (per batch sample) of a well-characterized, aged [242]Pu(IV)O$_2$(am,hyd) solid phase. Redox conditions were either buffered with 2 mM hydroquinone (HQ) at (pe + pH$_m$) ~ 10 or with Sn(II) at (pe + pH$_m$) ~ 1.5. Three series of solubility experiments were performed at $8 ≤ pH_m ≤ 13$: i. absence of ISA, ii. presence of ISA with 10^{-6} m ≤ m(ISA)$_{tot}$ ≤ 0.1 m, and iii. presence of ISA and Ca(II) with 10^{-6} m ≤ m(ISA)$_{tot}$ ≤ 0.1 m and 3·10^{-4} m ≤ m(Ca)$_{tot}$ ≤ 0.02 m. Solid phases retrieved from selected batch samples were characterized by XPS, in-situ XRD and Pu L$_{III}$ edge XANES/EXAFS at the INE-Beamline for Actinide Research at ANKA synchrotron facility.

Pu(III/IV)-ISA system. A pronounced increase of Pu(IV) solubility (compared to ISA-free systems) by up to 2.5 log$_{10}$-units was observed in the presence of ISA and absence of Ca(II) (see Figure 5). In HQ systems, slope analysis of solubility data in combination with solid phase characterization and DFT calcula-
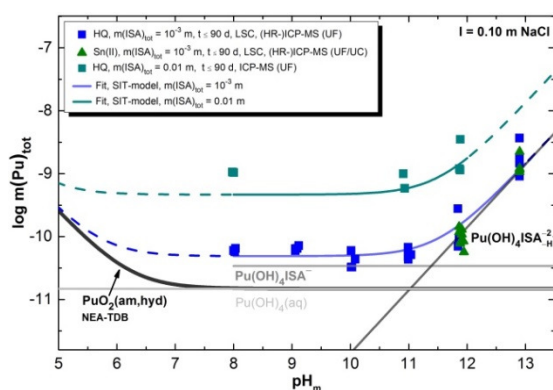
Fig. 5: Plutonium concentration in equilibrium with PuO$_2$(am,hyd) in redox buffered systems (■: hydroquinone; ▲:SnCl$_2$) at constant m(ISA)$_{tot}$ (0.01 m and 10^{-3} m). Solid lines correspond to the calculated solubility of PuO$_2$(am,hyd) in the absence of ISA: black line [6] and at constant m(ISA)$_{tot}$ = 0.01 m: dark green lines and 10^{-3} m: blue lines, using the thermodynamic model derived in this work.
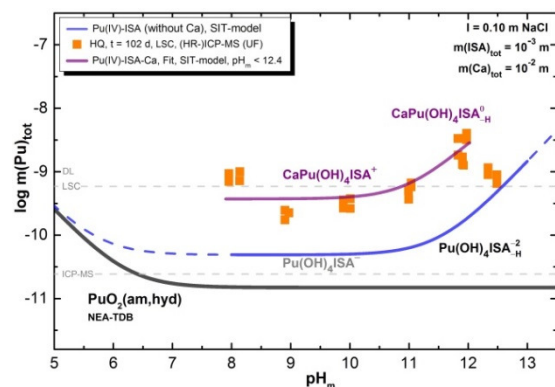
Fig. 6: Plutonium concentration in equilibrium with PuO$_2$(am,hyd) for HQ-buffered systems (■) at constant m(ISA)$_{tot}$ (10^{-3} m) and m(Ca)$_{tot}$ (0.01 m). Solid lines correspond to the calculated solubility of PuO$_2$(am,hyd) in the absence of ISA: black line [6]; with constant m(ISA)$_{tot}$ = 10^{-3} m: blue lines; and with constant m(ISA)$_{tot}$ = 10^{-3} m and m(Ca)$_{tot}$ = 0.01 m concentrations: purple line, using the thermodynamic model derived in this work.

tions resulted in chemical and thermodynamic models including the predominance of Pu(OH)$_3$ISA$_{-H}^-$ and Pu(OH)$_3$ISA$_{-2H}^{2-}$ complexes below and above pH$_m$ ≈ 12, respectively (with ISA$_{-H}$ and ISA$_{-2H}$ corresponding to ISA molecules where 1 and 2 alcohols groups are deprotonated). The significantly higher m(Pu)$_{tot}$ measured in Sn(II) systems with pH$_m$ < 12 indicated the formation of Pu(III)-ISA complexes under these boundary conditions. Above this pH$_m$, solubility data in HQ and Sn(II) systems were virtually identical indicating that the same equilibrium reaction (e.g. Pu(IV)(s) ⇔ Pu(IV)-ISA(aq)) controlled the solubility in both systems.

Ca(II)-Pu(III/IV)-ISA system. The presence of Ca(II) and ISA further enhanced the solubility of Pu in HQ-buffered systems (compared to Ca(II)-free systems), indicating the formation of quaternary Ca(II)-Pu(IV)-OH-ISA aqueous complexes (Figure 6). Chemical and thermodynamic models were derived for this system based on the slope analysis of solubility data and solid phase characterization, and included the formation of the quaternary complexes CaPu(OH)$_3$ISA$_{-H}^+$ and CaPu(OH)$_3$ISA$_{-2H}$(aq) below and above pH$_m$ ≈ 11, respectively. The proposed model overestimates the experimentally measured solubility at pH$_m$ ≥ 12.5 and m(ISA)$_{tot}$ ≥ 0.01 m, possibly due to the formation of a yet undefined Ca(II)-Pu(IV)-ISA solid phase. On the contrary, data collected in Sn(II)-buffered solubility experiments do not support the existence of analogous Pu(III)-bearing quaternary species with Ca(II) ions. The chemical and thermodynamic models derived in this work for the system Pu^{3+}-Pu^{4+}-Ca^{2+}-H$^+$–Na$^+$-ISA$^-$ -Cl$^-$-OH$^-$-H$_2$O(l) can be implemented in geochemical models/calculations, and provide relevant data for the safety analysis of repositories for the disposal of L/ILW.

- 14 -
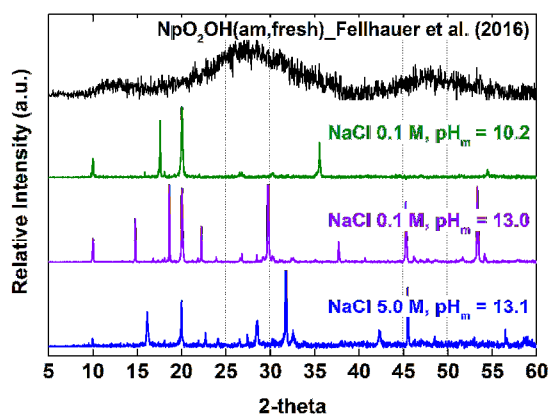
Fig. 7: *XRD patterns of Np(V) solid phases tempered at T = 80°C for 30 days in 0.1 and 5.0 M NaCl solutions. XRD diffractrogram reported in Fellhauer et al. (2016) [9] for NpO$_2$(am,fresh) is appended for comparison.*

Actinide solution chemistry at elevated temperatures

Temperature is one of the parameters that will vary during the different phases of operation of a high level radioactive waste (HLW) repository. Elevated temperature conditions (up to 200°C depending on hostrock system and repository concept) will affect actinide chemistry in the near-field of a HLW repository. In the context of the ThermAc project funded by BMBF, experiments on the solubility and the stability of solid phases of different actinides in aqueous solutions (NaCl, MgCl$_2$, CaCl$_2$) at T = 25 - 80°C were performed by KIT-INE.

The effect of temperature on Np(V) solid phase formation was investigated to obtain insights about the thermodynamic stability of Np(V) solid phases, assess the role of kinetics in solid phase transformations and evaluate possible redox processes occurring at elevated temperatures. About 5 mg of NpO$_2$OH(am,fresh) were equilibrated with 20 ml of various background electrolytes (0.1 and 5.0 M NaCl; 0.02, 0.15, and 3.5 M CaCl$_2$; 0.01 and 2.0 M MgCl$_2$) under Ar atmosphere. Initial pH$_m$ values in the solutions were between 6 and 13. Samples were tempered at T = (80 ± 5)°C for 30 days in airtight autoclaves. After cooling down to ambient temperature, Np solid phases were washed with ethanol for further analyses by means of powder X-ray diffraction (XRD), scanning electron microscopy combined with energy-dispersive X-ray spectroscopy (SEM-EDS), and quantitative analysis methods (ICP-MS/OES).

Apparent changes in color of Np(V) solids from initial green to either bluish-green, black, or violet, respectively, along with a considerable decrease in Np(V) solubility were observed in most of the tempered samples, unambiguously indicating the transformation of initial NpO$_2$OH(am,fresh) solid phases. Furthermore, a significant decrease of pH$_m$ values occurred which could be elucidated by the transformation into further hydrolyzed solid Np(V) phases.

Figure 7 represent the powder XRD patterns obtained for NaCl samples. In contrast to the initial amorphous NpO$_2$OH(am,fresh) [9], Np(V) solid phases tempered in alkaline NaCl solutions show characteristic XRD peaks indicating the formation of (micro)crystalline compounds.

The transformation of the initial Np(V) solid phase was also observed in CaCl$_2$ solutions. While a (micro)crystalline compound formed at weakly alkaline conditions, XRD patterns obtained for hyper-alkaline samples show the presence of rather poorly crystallized products, similar to CaNpO$_2$(OH)$_{2.6}$Cl$_{0.4}$·2H$_2$O(s) [9]. Although none of the collected diffractograms matched with that of crystalline NpO$_2$, the possibility of temperature induced redox transformations as reported in [10] will be further assessed by XANES/EXAFS at the INE-Beamline at ANKA synchrotron facility.

The result of the present work contributes to a better understanding of the solubility behavior and solid phase speciation of actinide elements, and provides relevant process understanding for the reliable Safety Assessment of high-level waste repositories in deep-geological formations.

Complexation of Cm(III) with malonate

Small organic molecules are present naturally in ground waters or can be formed due to degradation of macromolecular organic matter (e.g. humic/fulvic acids). The complexation of actinides with small organic ligands is a topic of fundamental scientific interest and a potentially relevant geochemical process and may influence the migration behavior of actinides in a potential host-rock of a nuclear waste repository. Detailed thermodynamic data at ambient and elevated temperatures as well as structural information of the different complexes are necessary for an in-depth understanding of the complexation mechanism on the molecular level.

In the present work, the complexation of Cm(III) with malonate is investigated by time resolved laser fluorescence spectroscopy as function of [Mal^{2-}]$_{tot}$, I_m(NaCl) and T = 20 - 90°C, and evaluated using the specific ion interaction theory (SIT) as performed for
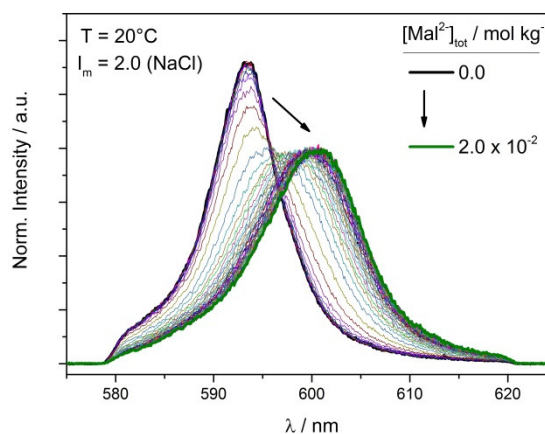
Fig. 8: *Emission spectra of Cm(III) (10^{-8} m) as function of [Mal^{2-}]$_{tot}$. T = 20 °C, I_m = 2.0 m (NaCl).*

comparable ligand systems [11-12]. Furthermore, the structures of the respective complexes are determined by quantum chemical calculations.

The evolution of the fluorescence spectrum of Cm(III) with the total concentration of malonate is shown in Figure 8. The emission band of the Cm^{3+} aquoion (593.8 nm) is clearly shifted towards 601 nm with increasing $[Mal^{2-}]_{tot}$. This is attributed to the successive shift of the Cm(III) speciation towards complexed species. Using the SIT, the log $K^0_n(T)$ of the $[Cm(Mal)_n]^{3-2n}$ complexes (n = 1, 2) were determined for the entire temperature range. The log $K^0_3(T)$ was determined only for $T \geq 40$ °C. The results show a general increase of the constants with the temperature by about 0.25 - 0.50 orders of magnitude.

The stability constants are linearly correlated with the reciprocal temperature. Thus, their temperature dependency is fitted by the integrated Van't Hoff equation, yielding the respective thermodynamic functions $\Delta_r H^0_m$ and $\Delta_r S^0_m$ of the complexes. The results show a small and almost constant reaction enthalpy around 10 kJ·mol^{-1} for each stepwise formation of the three complexes. The reaction entropies however decrease successively for each complexation step from 130 to 60 J·mol^{-1}K^{-1}.

This effect is explained by analyzing the calculated structures of the different Cm(III) malonate species. For each complex, every combination of end-on (non-chelating) and side-on (chelating) coordination is calculated and the respective binding energies (BE) are compared. The lowest BE are found for the structures with only side-on coordinated ligands, showing that malonate prefers a chelating binding mode to Cm(III) via two oxygen atoms, one of each carboxylic group. This is in agreement with the analogues ligands oxalate and succinate [11-12]. Contrary to these two ligands however, for malonate the difference between the BEs of the all side-on structures to the mixed structure with one ligand in end-on coordination are quite small. The reason is that the length of the carbon chain of malonate enables the ligand to form hydrogen bonds to inner-sphere water molecules of Cm(III) via the free carboxyl group when in end-on coordination. This stabilizes the end-on coordination of malonate to some extent and lowers the respective BEs. To illustrate this effect, the structure of $[Cm(Mal)_{2,side}(Mal)_{end}]^{3-}$ complex is given in Figure 9.

The present work gives detailed insights into the complexation of Cm(III) with malonate, showing how structural properties of the ligand influences the coordination on the molecular level, which in turn affects
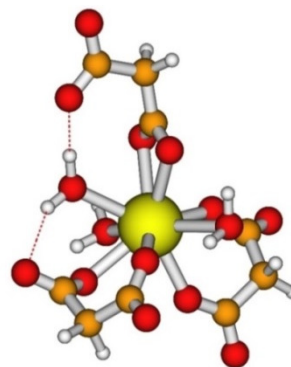
Fig. 9: *Molecular structures of $[Cm(Mal)_3]^{3-}$ with two ligands coordinated side-on and one ligand end-on.*

the thermodynamics of complexation on the macroscopic scale. The results contribute to an in-depth understanding of the interaction of aliphatic dicarboxylic ligands with trivalent actinides in aqueous solution.

References

[1] Guillaumont, G., et al., *Chemical Thermodynamics Vol. 5*, Elsevier, Amsterdam, (2003).

[2] Yalcintas, E., et al., Dalton Transactions, **45**, 8916–8936, (2016).

[3] Alliot, I., et al., Environ. Sci. Technol., **43**, 9174–9182, (2009).

[4] Neck, V., et al., Radiochim. Acta, **89**, 1-16, (2001).

[5] Almkvist, L. and Gordon, A., *Low and intermediate level waste in SFR 1. Reference waste inventory 2007*. SKB R-07-17, Svensk Kärnbränslehantering AB, (2007).

[6] Neck, V., et al., C. R. Chimie, **10**, 959-977, (2007).

[7] Glaus M.A., et al., Environ. Sci. Technol., **42**, 2906-11, (2008).

[8] Gaona, X., et al., J Contam Hydrol, **102**, 217-27, (2008).

[9] Fellhauer, D., et al., Radiochim. Acta, **104**, 381-397, (2016).

[10] Roberts, K. E., et al., Radiochim. Acta, **91**, 87-397, (2003)

[11] Skerencak-Frech, A. et al., Inorg. Chem., **54**, 1860-1868, (2015).

[12] Fröhlich, D.R., et al, Inorg. Chem., **55**, 4504-4511, (2016).